

Rocking curve measurements revisited

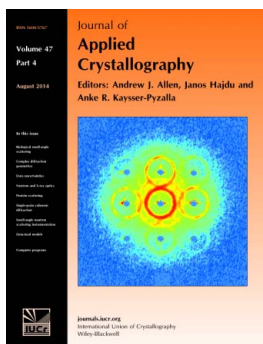
Fabio Masiello, Gianfranco Cembali, Alexander I. Chumakov, Simon H. Connell, Claudio Ferrero, Jürgen Härtwig, Ilya Sergeev and Pierre Van Vaerenbergh

J. Appl. Cryst. (2014). **47**, 1304–1314

Copyright © International Union of Crystallography

Author(s) of this paper may load this reprint on their own web site or institutional repository provided that this cover page is retained. Republication of this article or its storage in electronic databases other than as specified above is not permitted without prior permission in writing from the IUCr.

For further information see <http://journals.iucr.org/services/authorrights.html>



Many research topics in condensed matter research, materials science and the life sciences make use of crystallographic methods to study crystalline and non-crystalline matter with neutrons, X-rays and electrons. Articles published in the *Journal of Applied Crystallography* focus on these methods and their use in identifying structural and diffusion-controlled phase transformations, structure-property relationships, structural changes of defects, interfaces and surfaces, *etc.* Developments of instrumentation and crystallographic apparatus, theory and interpretation, numerical analysis and other related subjects are also covered. The journal is the primary place where crystallographic computer program information is published.

Crystallography Journals **Online** is available from journals.iucr.org

Rocking curve measurements revisited

Fabio Masiello,^{a*} Gianfranco Cembali,^a Alexander I. Chumakov,^{b*} Simon H. Connell,^{c*} Claudio Ferrero,^{b*} Jürgen Härtwig,^{b,c*} Ilya Sergeev^d and Pierre Van Vaerenbergh^b

^aPANalytical BV, Lelyweg 1 (7602 EA), Almelo, 7600 AA, The Netherlands, ^bESRF – The European Synchrotron, 71 avenue des Martyrs, CS 40220, Grenoble 38000, France, ^cPhysics, University of Johannesburg, cnr Kingsway Avenue and University Road, Johannesburg 2092, South Africa, and ^dHASYLAB at DESY, Notkestrasse 85, Hamburg 22607, Germany. Correspondence e-mail: fabio.masiello@panalytical.com, chumakov@esrf.fr, simonhconnell@gmail.com, ferrero@esrf.fr, haertwig@esrf.fr

In order to correctly analyse high-resolution rocking curves of high-quality crystals, a special effort is needed to estimate the systematic contributions coming from the experimental setup. This article highlights the main areas that require special analytical treatment and presents results obtained using different approaches to the problem, as well as some typical results for high-quality silicon and diamond crystals.

© 2014 International Union of Crystallography

1. Introduction

The study of materials by diffraction methods started about 100 years ago with the pioneering experiment of Laue, Friedrich and Knipping, when the first X-ray diffraction patterns of single crystals were obtained (Friedrich *et al.*, 1912). This was the beginning of a rapid development fostering many diffraction-based methods and techniques, which is still continuing. The measurement of rocking curves and the associated derived quantitative parameters, such as the ‘full width at half-maximum’ (FWHM) of the curves, has been performed since at least 1921 (Davis & Stempel, 1921) by exploiting the X-ray diffraction (XRD) properties of crystals. Since then, this has become one of the most powerful methods for the diffraction-based characterization of crystalline materials. The experimentally closely related method of X-ray diffraction imaging or X-ray diffraction topography has been used since about 1931 (Berg, 1931). Soon after World War II, the requirements of the electronics industry for the nondestructive analysis of defects in semiconductor materials like silicon and germanium (and others) boosted the improvement of these methods to their modern high-resolution variants like high-resolution X-ray diffraction and in particular high-resolution and high strain sensitivity X-ray topography (Bond & Andrus, 1952; Lang, 1957). This evolution was additionally accelerated in the late 1970s by the use of synchrotrons as dedicated X-ray sources and later on, starting in the 1990s, by the use of third-generation synchrotron sources.

The measurement of X-ray rocking curves is a rather simple and fast integral method which provides characteristic quantitative values. The broadening of the FWHM is primarily due to the presence of defects and other imperfections in the crystals (or on their surfaces). This means that it depends directly on the crystal quality. By controlling the dimensions of the X-ray beam by slits, it is possible to collect this averaged information from the complete sample or from local areas of

different size. It appears that this kind of measurement is particularly well suited to studying samples of lower quality. However, the better the crystal quality, the less efficient this method becomes and the more problems appear in the data analysis. The origin of the problems is that the broadening of the rocking curve may be well below the theoretical FWHM of the reflectivity curve of a perfect crystal (in short called the ‘Darwin width’, but more precisely it should be called the Prins–Darwin width). For crystals like silicon or diamond (and in the case of strong reflections or hard X-rays) this effect may occur for FWHMs of the order of or below one arcsecond.

One may get the impression that for this classical and well established method all is known and there is nothing new to learn from it. However, when dealing with high-quality samples for X-ray optical applications with high-quality X-ray beams, it is necessary to extend this method to its limits. Our aim was to study the degree of crystal quality that it may be possible to quantitatively characterize reliably by measuring the broadening of the rocking curve of a crystal containing defects compared to that of a perfect crystal. Several issues were encountered, indicating that there is still much to be learned with regard to high-precision rocking curve measurements.

The present study is based on two experimental goals. The first is the characterization and quantification of the surface quality of silicon crystals after different surface processing treatments. The second is the determination of the contributions to the rocking curve broadening from both the bulk and the surface defects in synthetic diamonds. Silicon and diamond are very important materials used to manufacture X-ray optical elements (like simple monochromators, beam-splitter monochromators or phase plates) for beamlines at (high-energy) synchrotron light sources and free-electron lasers. Of course, rocking curve measurements were not the only means utilized to study the material bulk and the surface processing

quality for these applications. In addition, we extensively used X-ray diffraction topography (Burns *et al.*, 2009; Masiello, 2011).

2. Some basics

In analogy to classical optics, we define the reflectivity (R_h) or ‘reflectivity curve’ of a perfect crystal as the dependence of the power diffracted by that crystal on the incident angle of a plane and monochromatic X-ray wave. This may be calculated using the formulas from the dynamical theory of X-ray diffraction from perfect crystals. The ‘reflectivity curve’ of a perfect crystal is a theoretical response function for the diffraction of a plane monochromatic wave by that crystal. It is a theoretical limit that may only be approached in an experiment by using dedicated X-ray optical experimental conditions to measure rocking curves. We define the ‘rocking curve’ of a real crystal (this may be a nearly perfect crystal or a crystal with defects) as a rather complicated multiple integral containing both the reflectivity curve of that crystal and the ‘instrument response function’, also called ‘instrumental broadening’ or ‘apparatus function’, depending on spatial, angular and energy coordinates. The apparatus function contains all geometrical, angular and spectral properties of the radiation emitted by the source and modified on its pathway to the crystal by the entire optical system (filters, slits, other crystals *etc.*) (Azároff, 1974; Härtwig & Grosswig, 1989; Härtwig *et al.*, 1993). The first reflectivity curve was simulated very early on by C. G. Darwin in 1914 (Darwin, 1914), just after the discovery of the diffraction of X-rays by crystals. The first experimental curve that approached the theory was published only in 1962 by Bubáková (1962). In most cases (see Härtwig *et al.*, 1993, and citations therein) a rocking curve is, to a good approximation, just the convolution of the reflectivity curve and the apparatus function, and we consider this valid within the scope of this work.

To separate explicitly the broadening of the crystal reflectivity curve due to the presence of defects, we assumed a rather general case (as used in line profile analysis) where the experimental rocking curve of a high-quality yet defective single crystal is the result of the convolution of three curves (Fig. 1). These are, firstly, the reflectivity curve of a perfect crystal, secondly, the instrumental broadening represented by the apparatus function, which takes into account all contri-

butions from the optical elements conditioning the beam impinging on the sample, and, thirdly, the broadening due to crystal defects, which is the effect produced by the presence of defects in the bulk of the crystal, as well as defects on its surface and in the subsurface region. The difficulty in the case of crystals with rather high quality is at least twofold. In the first place, as known from information theory, for precise results the apparatus function should be well known and as narrow as possible (as close as possible to a δ function), something that is often not easy to achieve in practice. In the second place, the broadening due to defects may be narrower than the width of the reflectivity curve itself. This poses considerable problems in numerical fitting and de-convolution procedures. In addition, one has to remember that the FWHM as a characteristic parameter is not sufficient for a reliable description of the influence of crystal bulk and subsurface defects on the broadening of a rocking curve. The whole rocking curve (including the wings far away from the maximum) contains important information and has to be measured and taken into account in the analysis. Its maximum position and in particular the detailed shape may strongly depend on local variations of lattice parameters and lattice tilts (diagonal and off-diagonal components of the strain tensor). This is due to the presence of defects in the crystal volume, contributing to the (integrated) diffracted intensity and proportional to the extinction depth of the X-rays in the crystal. The height of the wings is known to be influenced by the diffuse scattered radiation. In order to extract the effect of crystal imperfections from a measured rocking curve, it is necessary to separate their contributions from the reflectivity curve of a perfect crystal as well as from the apparatus function. The reflectivity curve is known with high precision from the dynamical theory of X-ray diffraction; however, the apparatus function must be determined experimentally and/or theoretically with high precision.

3. Experimental

In order to use rocking curve measurements for characterizing high-quality crystals foreseen as Bragg diffracting optical elements, one has to achieve high strain sensitivity. Additional effort has to be expended to decrease the width of the apparatus function as much as possible and determine its form with the utmost accuracy. This suggests a nondispersive config-

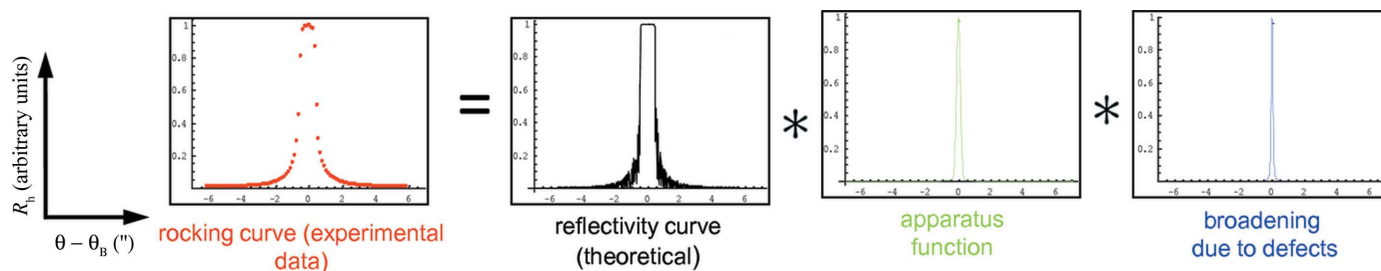


Figure 1

Pictorial example of a rocking curve, assumed to be the convolution of three distinct curves: the reflectivity curve (theoretical), the apparatus function and a function describing the broadening due to defects *via* an integral expression. Experimental data were obtained on a high-quality Ila HPHT diamond crystal, 400 reflection, $E = 14.413$ keV.

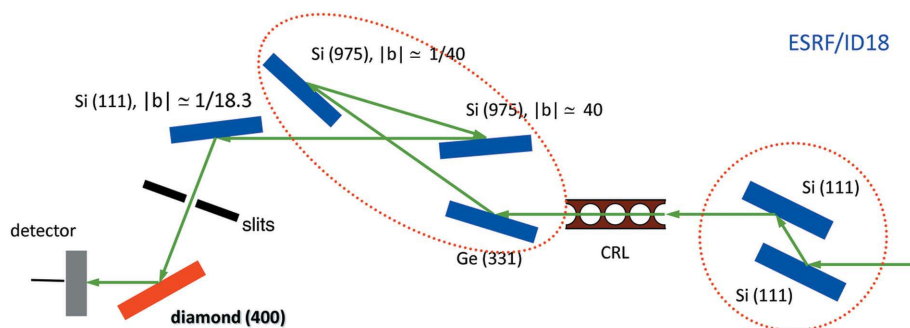


Figure 2

ID18 experimental configuration used for high-resolution X-ray diffractometry of synthetic diamonds. From the right to the left one sees a silicon double-crystal pre-monochromator (red circle), a set of compound refractive lenses (CRL), a three-crystal very high energy resolution monochromator (red ellipse) and an asymmetrically cut silicon collimator, followed by the slits, the sample and a detector/counter.

uration, which can be obtained in at least three different fashions:

(1) Using an $(n, -n)$ double-crystal geometry, where the same material and the same reflection are used for both sample and beam-conditioning (monochromator) crystals (Bond & Andrus, 1952; Burns *et al.*, 2009).

In that case it is advantageous to use the monochromator crystals in asymmetric geometry with grazing incidence. The bulk and surface quality of these crystals must be close to perfect, thus severely reducing the range of applicability of this approach to a few high-quality crystals. We used such a popular and rather simple configuration, consisting of an asymmetrically cut silicon monochromator (to obtain a good collimation) and symmetrically cut samples, for our studies of silicon processing (see §5.1). For our purpose this was enough to obtain the desired resolution.

We did not use this kind of setup to investigate the quality of synthetic diamond for the simple but very important reason that in the early phase of these studies we had no diamond plates with large enough perfect areas. They were not (yet) usable as perfect collimator–monochromator crystals. The background to our studies was just to help crystal growers to produce high-quality crystals (Burns *et al.*, 2007).

(2) Reducing the wavelength spread by using a high-resolution monochromator, combined with an (asymmetrically cut) collimator crystal.

We used this configuration at the nuclear resonance beamline ID18 (Rüffer & Chumakov, 1996) of the ESRF (energy resolution $\Delta E/E = 3 \times 10^{-8}$) and carried out crystal quality measurements. For this purpose we added an asymmetrically cut collimator crystal to also reduce the beam divergence. In this way, we studied silicon crystals after different crystal processing steps, as well as diamond plates with different crystal growth histories and/or different crystal surface processing procedures. Most rocking curve measurements, in particular the diamond ones, were done with this configuration (see Fig. 2).

(3) Using a bendable monochromator, which is able to locally adapt the Bragg angle (Altin *et al.*, 2002) to that of the investigated samples and thus to obtain a nondispersive

geometry even though different crystal materials and/or reflections are employed.

This approach was mainly used for the study of diamond plates by X-ray diffraction imaging and rocking curve imaging, with the aim of measuring very low residual strains in nearly defect-free samples (Masiello, 2011). The classical rocking curve measurements were in this case mainly meant for the sample adjustment.

For completeness it is worth mentioning that it is possible to use also so-called quasi-nondispersive configurations. In this case, the two flat crystals in the double-crystal setup (case 1

above) may be made of different materials, but the used reflections must exhibit very similar values of the lattice plane distances (d spacing) and therefore also similar Bragg angles. This configuration was, for example, used by Sellschop *et al.* (2000). However, in this case the resulting rocking curves suffer an additional broadening due to dispersion, which decreases along with decreasing differences of the Bragg angles. This additional broadening must be determined for high-accuracy measurements.

The rather general theoretical approach mentioned above (whereby the experimental rocking curve is modelled as a convolution of three curves) is well adapted to analyse results from all the three configurations described above.

Since most of the rocking curve measurements, in particular those referring to diamond crystals, were conducted at the ESRF nuclear resonance beamline ID18, we present here one of the standard layouts we used (Fig. 2). The most often used X-ray energy was 14.413 keV.

4. Main problem – determination of apparatus functions

It is possible to describe the effect of the instrumental broadening by a convolution integral:

$$e(t) = \int_{-\infty}^{\infty} f(\tau)i(t - \tau) d\tau \stackrel{\text{def}}{=} (f * i)(t). \quad (1)$$

The function $f(t)$ represents the theoretical apparatus function one attempts to measure. The function $e(t)$ is the measured rocking curve, *i.e.* the weighted average over $i(t)$ of the true curve $f(t)$.

We decided to determine the apparatus function both theoretically and experimentally. Actually, three different methods have been used for evaluating the apparatus functions:

- (1) Theoretical approach – direct calculation
- (2) Experimental approaches –
 - (2.1) extrapolation *via* a model function
 - (2.2) direct deconvolution

4.1. Theoretical approach – direct calculation

The calculation of the apparatus function was performed using a program written by one of the authors (GC) (Masiello, 2011). This program works out the apparatus function by taking into account all the optical elements present on the beamline (slits, monochromators, compound refractive lenses). The overall curve, as obtained downstream from the sixth crystal in Fig. 2, has an FWHM of $0.037''$. It is important to highlight that this estimation is done without taking into account any imperfection in the system. It is therefore to be considered as a theoretical lower limit of the real apparatus function.

4.2. Experimental approaches

4.2.1. Model and fit approach. In order to measure the apparatus function it would be necessary to sample the incoming beam (measure the rocking curve) with a δ -shaped reflectivity curve, obtaining in the instrument response the apparatus function itself. This is impossible, but one can approximately model the actual situation. Firstly, one has to use an analyser crystal the perfection of which is such that one may ignore the broadening due to defects. Secondly, it is possible to approach a δ function in a stepwise fashion by measuring the incoming beam by means of different reflections with decreasing Darwin widths associated with this 'perfect' sample, in our case a well processed 111 1 cm-thick silicon sample. The apparatus function analysis has been carried out in two independent ways: in the first, the apparatus function has been fitted *via* a model curve with a set of free parameters; in the second, direct deconvolution algorithms have been used. One of the most serious problems in both methods has been the fact that the apparatus function from the optical system installed at ID18 is indeed very narrow, thanks to the high beam collimation and energy resolution. To extract tiny broadenings from a series of measured rocking curves is therefore a complicated task.

The apparatus function was modelled by the sum of a Gaussian and a Lorentzian function [similar to a pseudo-Voigt

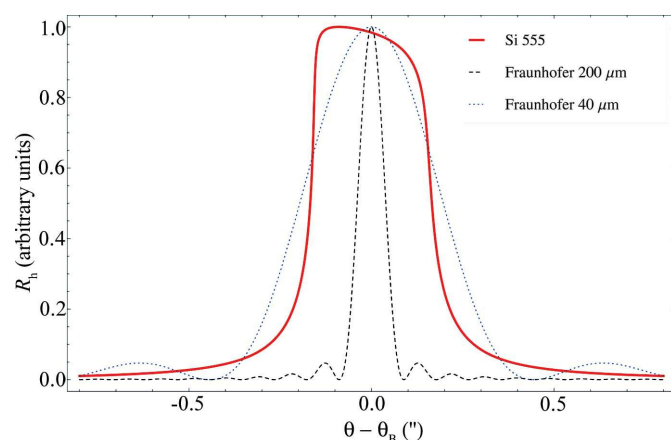


Figure 3

Comparison of the Si 555 reflectivity curve ($E = 14.413$ keV) with the Fraunhofer diffraction pattern at the sample position from rectangular slits with aperture 200 and $40 \mu\text{m}$.

curve, often used in the description of a diffraction peak shape, for example by Ida *et al.* (2000)]:

$$\text{app}(\Delta\theta) = A_L \frac{2}{\pi} \frac{\omega}{4\Delta\theta^2 + \omega^2} + A_G \frac{1}{\sigma(2\pi)^{1/2}} \exp\left(-\frac{\Delta\theta^2}{2\sigma^2}\right), \quad (2)$$

where A_L and ω are the area and the FWHM, respectively, of the Lorentzian term, and A_G and σ are the area and standard deviation, respectively, of the Gaussian term. These four parameters are used as free model parameters. The code was written in *Mathematica* (Wolfram Research, 2009) and uses the GlobalSearch algorithm within the *Global Optimization 6.0* package (<https://www.wolfram.com/products/applications/globalopt/manual.pdf>) to minimize the difference between experimental data and the convolution of the apparatus function with the theoretical reflectivity. Owing to the large number of convolution integrals required in this procedure, the code is quite slow. Equation (2) was used for all results mentioned in this section.

The first result of the data analysis was the characterization of the dependence of the apparatus function on the size of the vertical slits upstream from the sample. The Fraunhofer diffraction from the slits plays an important role in such a high-resolution experiment, entailing sub-arcsecond distortions, even if the slits are as large as $200 \mu\text{m}$ (Fig. 3). This also shows that the slits in front of the sample were not a good means to measure local rocking curves; however, there is no problem when using widely open slits and in this way integrating information over the entire sample width.

The first attempt to solve this problem was to include the Fraunhofer diffraction from the slits as an additional broadening of the theoretical reflectivity curve. The results were not satisfactory, especially for slit apertures of less than $100 \mu\text{m}$. We thus decided to include the diffraction from the slits in the apparatus function. In this way, all identifiable additional

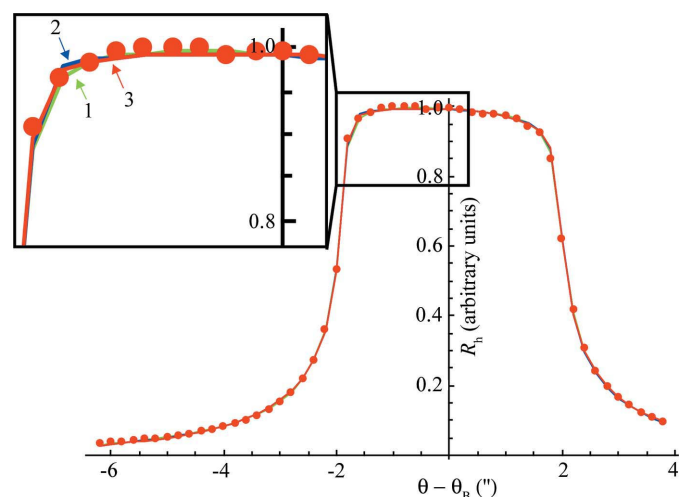


Figure 4

Scan over a narrow angular range. Comparison between the experimental data (Si 111 reflection; red points) and the fits (curve 1 green, curve 2 blue, curve 3 red lines) with three different apparatus functions (Fig. 5). Inset: a zoom of the region indicated in the black rectangular frame, showing that the three solutions are equally good.

Table 1

The fit parameters for the curves labelled 1, 2, 3 in Fig. 5.

Curve	A_L (%)	A_G (%)	ω (")	σ (")
1	82.7	17.3	0.03	169.9
2	13.6	86.4	3.47	0.23
3	6.3	93.7	2.67	0.11

effects, such as diffuse scattering, small-angle scattering or the non-ideal shape profile of the slits, are automatically included. Therefore, we worked with three different apparatus functions for the three slit sizes used in the experiments: 700, 200 and 40 μm .

The following task was to measure and analyse rocking curves using different reflections featuring decreasing Darwin widths. The initial fitting procedure was insufficiently constrained and different sets of fit parameters gave similar results. An example of this is given in Fig. 4. The experimental data (red points) collected in a rather narrow angular range around the maximum of the rocking curve (Fig. 4; the inset zooms into the region indicated) match equally well with the results obtained from the convolution of the reflectivity curve with the three different apparatus functions (Fig. 5). The fit parameters for each of the curves, labelled 1, 2 and 3 in Fig. 5, are displayed in Table 1. The problem that different sets of fit parameters gave very similar results was solved by collecting, in addition to the narrow scans, also experimental data *via* much broader scans (in the present case $\pm 25''$, the only limitation being the number of experimental data points used in the software) and by comparing them with the three functions in Fig. 5. To demonstrate this approach, two of the three results are shown in Figs. 6 and 7. The best result (and actually the only good one) shown in Fig. 7 is represented by the second curve from Fig. 5. The black line in Figs. 6 and 7 is the theoretical rocking curve (perfect crystal without defect contribution).

Finally, a series of apparatus functions was obtained for the different reflections used, namely 111, 333, 444 and 555

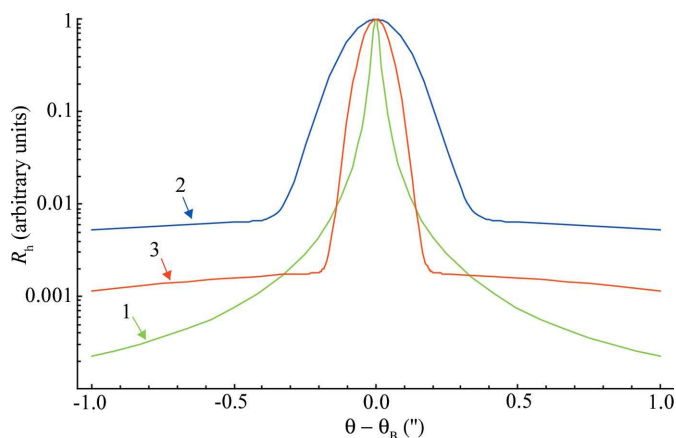


Figure 5

The three apparatus functions, plotted on a log scale over a narrow angular range. The fit parameters for each of the curves, labelled 1, 2, 3, are found in Table 1. The parameters and shapes are very different, but the quality of the fits is very similar.

symmetric Bragg reflections, which have the Darwin widths 4.04, 0.91, 0.69 and 0.30'', respectively. By extrapolating the results obtained towards a 'zero-width curve', *e.g.* for the 200 μm slit size (Fig. 8), we obtained the final three apparatus functions for the different vertical slits sizes used during the experiment, as displayed in Fig. 9 and Table 2. Most experiments were done with a slit size of 200 μm , as will be explained in §4.2.3.

4.2.2. Direct deconvolution methods. Direct deconvolution is well defined for continuous analytical functions. However, experimental data are available only as a discrete set of points in a restricted finite range with both systematic and statistical errors. A general feature of the deconvolution procedure in these cases is its ill-posedness, and the deconvolution algorithm based on equation (1) needs not have a unique solution (Jones & Misell, 1970). The practical implication of this property is that the solution of an integral equation may be

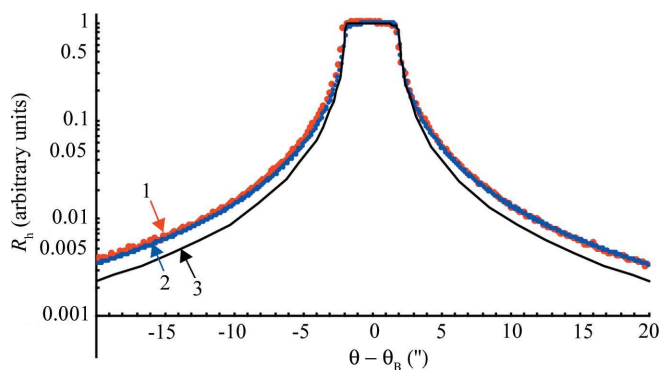


Figure 6

Comparison of the experimental data collected over a broader range ($\pm 25''$; curve 1 and red points) with the fit using the second curve shown in Fig. 5, which represents the best result (curve 2, blue line). For comparison the rocking curve calculated for a perfect crystal (without defect contribution) is shown as curve 3 (black line).

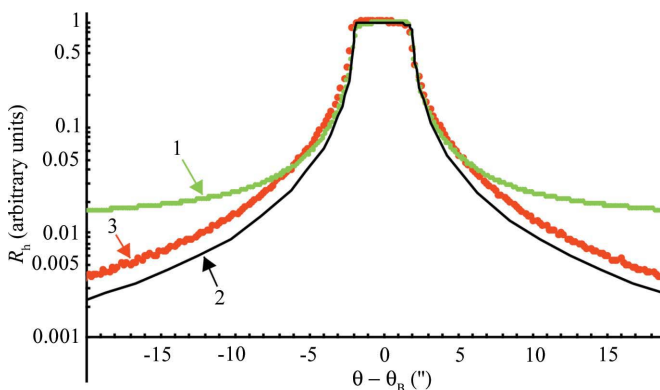


Figure 7

Comparison of the experimental data collected over a broader range ($\pm 25''$; red points) with the fit (shown by the green curve 1) using the apparatus function shown as the first curve in Fig. 5, which uses the parameters shown in Table 1 (fit labelled 1). The bad fit quality becomes evident on this angular scale. A similar poor result is obtained using the apparatus function shown in Fig. 5 as the red curve 3, which uses the parameters shown in Table 1 labelled 3. For comparison the rocking curve calculated for a perfect crystal (without any defect contribution) is shown in black (curve 2).

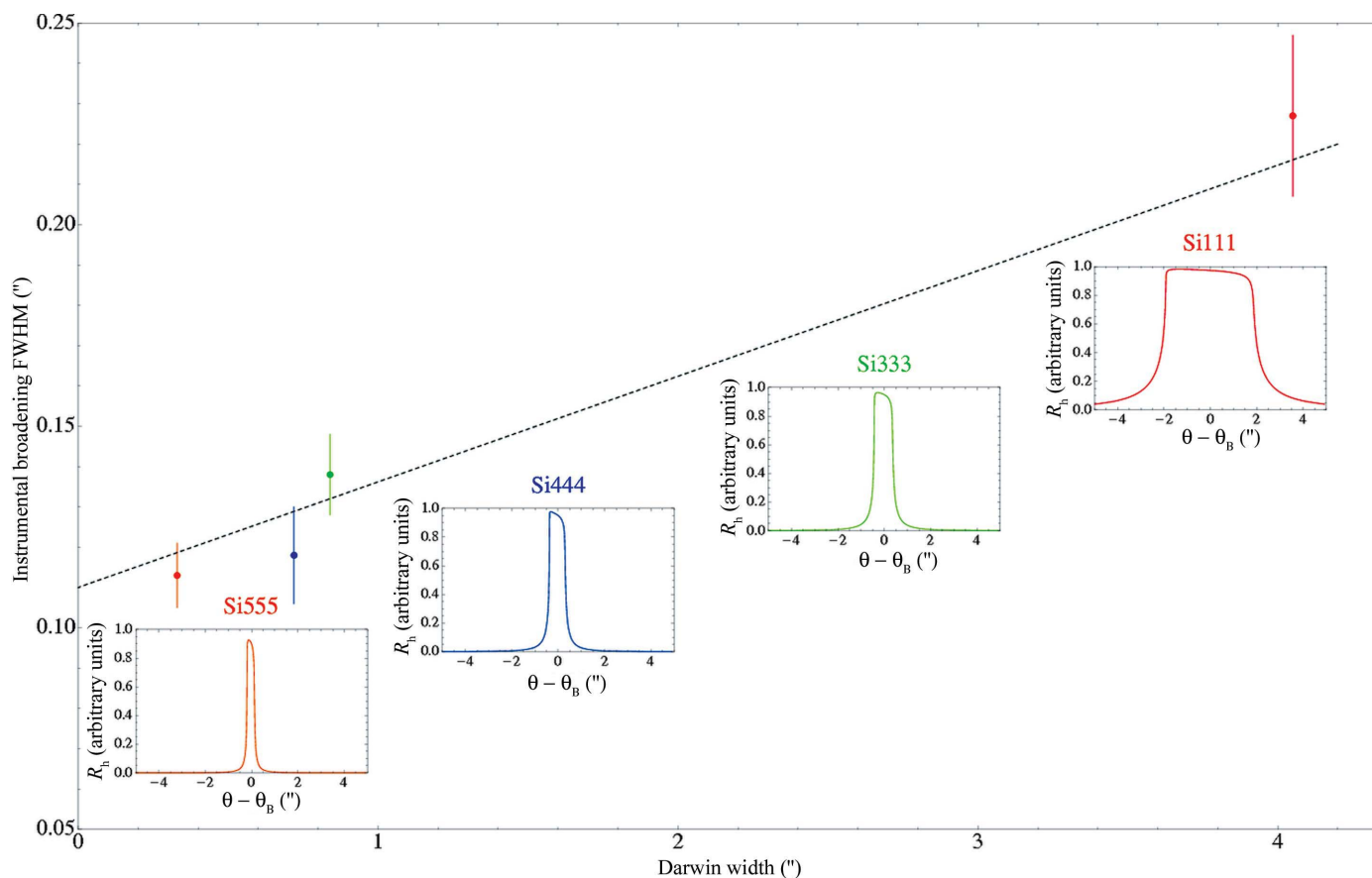


Figure 8 Extrapolation of the apparatus function towards a ‘zero-width’ curve, slit size 200 μm . The points with error bars represent the FWHM values for the apparatus function corresponding to the different reflections (111, 333, 444 and 555). The four insets show the related measured curves.

completely corrupted by an excess of noise propagation. Actually, deconvolution as applied to a digital data set is still a problem to work on for mathematicians. In order to tackle this issue and obtain reliable solutions, approximations are always necessary. In our case an implementation based on a *Mathematica* code that uses two different algorithms with several special features was employed. These algorithms are the Burger–Van Cittert (Burger & Van Cittert, 1932) and the Richardson–Lucy algorithms (Richardson, 1972; Lucy, 1974), applied in order to extract the apparatus function.

4.2.3. Comparison of the results obtained. In Fig. 10 the results obtained with the above-mentioned and other different deconvolution methods are presented. We show the case of a slit of 200 μm size, which was used in most experiments. This slit size is the result of a reasonable compromise between moderate diffraction effects on the slits (the slit gap should not be too narrow – see the discussion in §4.2.1 and the illustration in Fig. 3) and the dimensions of the beam footprint on the sample in order to have also rather local information. This choice gave the best results when analysing the diamond crystals, which may display regions with both higher and lower quality. For the wider slit apertures (700 μm) the footprint on the sample was ~ 1.5 mm for the Si 400 reflection and ~ 3.4 mm for the Si 111 reflection. These values were too large, because the high- and low-quality regions of the crystals were

measured at the same time. For the narrower slit gaps (70 μm), the Fraunhofer diffraction from the slits may be larger than the ‘broadening due to defects’, which is the effect that we are interested in, and this fact could complicate the data analysis by considerably increasing the width of the related apparatus function.

As discussed previously, the direct calculation provides the narrowest curve for the apparatus function, *i.e.* a theoretical lower limit for the case that no imperfections are present in

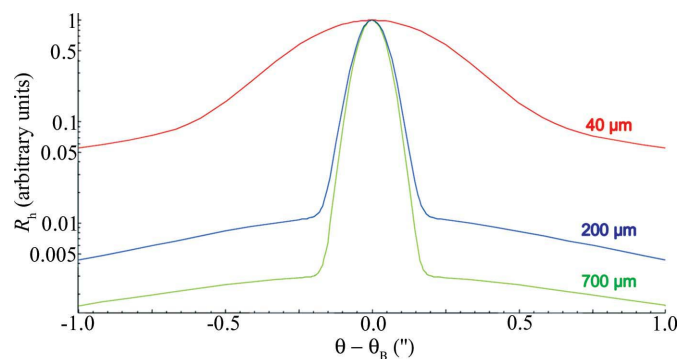


Figure 9 Plot of the global apparatus functions obtained for the three different vertical slit sizes. The fit parameters and the full widths at different heights (50, 20, 2%) for these vertical slit sizes are presented in Table 2.

Table 2

The fit parameters and the full widths at different heights (50, 20, 2%) for three vertical slit sizes.

Slit size (μm)	A_L (a.u.)	ω (")	A_G (a.u.)	σ (")	FWHM (")	FW20%M (")	FW2%M (")
700	0.006	2	0.07	0.045	0.11	0.16	0.26
200	0.008	1.5	0.035	0.05	0.12	0.18	0.31
40	0.045	2.6	0.06	0.23	0.58	0.93	4.23

the optical system, including the analyser crystal. It appeared that the results obtained with the Van Cittert deconvolution algorithm strongly depend on the different reflections used for the silicon analyser employed to measure the rocking curves to be deconvolved. This can be seen by deconvolving rocking curves measured for the same optical system, once with a silicon analyser crystal using the Si 333 reflection, with its rather wide intrinsic reflectivity curve (in angular scale), and once with a silicon analyser crystal using the Si 555 reflection, with its rather narrow intrinsic reflectivity curve. This should not be the case for a robust deconvolution method. However, when using the Richardson–Lucy algorithm the effect related to the analyser reflection was not present. Finally, the results obtained with the model fitting approach compare well with the direct deconvolution results obtained *via* the Richardson–Lucy method, and hence this method has been used for the rest of the analysis.

Another experiment was performed in order to obtain an even more accurate estimation of the apparatus function. This was done by using a different energy (23.879 keV, corresponding to the nuclear resonance of ^{119}Sn) in order to be able to use even higher order reflections, *i.e.* Si 777, Si 888 and Si 999, together with the quasi-forbidden Si 222 reflection. The idea behind this experiment was the same as the previous one, *i.e.* approaching by measuring reflectivity curves of higher-order Bragg reflections a δ -shaped function in order to be able to record only the apparatus function. The FWHMs for the allowed reflections, 777, 888 and 999, are 0.063, 0.062 and 0.033", respectively, whilst for the 222 forbidden reflection we found a value of 0.025" by using the structure factor value

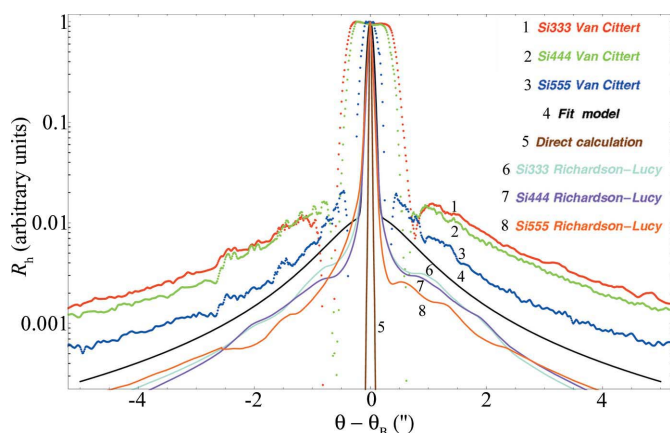


Figure 10

Comparison of the apparatus function obtained with the different methods.

1.456 determined experimentally by Alkire *et al.* (1982). Fig. 11 shows a comparison of the experimental data obtained with the different reflections together with the apparatus function obtained for a slit size of 200 μm, as well as the theoretical reflectivity curves for the different reflections (inset). This graph demonstrates that, even though the theoretical predictions (inset) indicate that the curves are getting narrower for increasing *hkl* reflection orders, the experimental rocking curves stay almost constant, *i.e.* the contribution of the used crystal reflection became negligible and we were measuring directly the apparatus function. Moreover, the agreement between the experimental data and the apparatus function determined above is very good, considering that the experimental conditions for the two cases were not the same. In conclusion, we are confident that the apparatus function determination by our measurements is accurate and allows a correct estimation of the broadening due to defects for the diamond samples.

5. Some typical results and discussion

As mentioned in the introduction, the object of this investigation is directly related to two classes/varieties of problems (Barrett *et al.*, 2010) in the context of developing improved X-ray optical elements at the ESRF. The first concerns the quantitative characterization of the surface quality of silicon crystals. The second concerns the precise characterization of high-quality synthetic diamonds. In particular, we concentrated on the reliable integral measurements of rocking curve broadenings due to bulk and surface defects in manufactured diamond plates.

5.1. Surface processing of silicon

Owing to the huge investments made in recent decades by the electronics industry (Zulehner, 2000), it is nowadays possible to produce silicon crystals both of a large size and

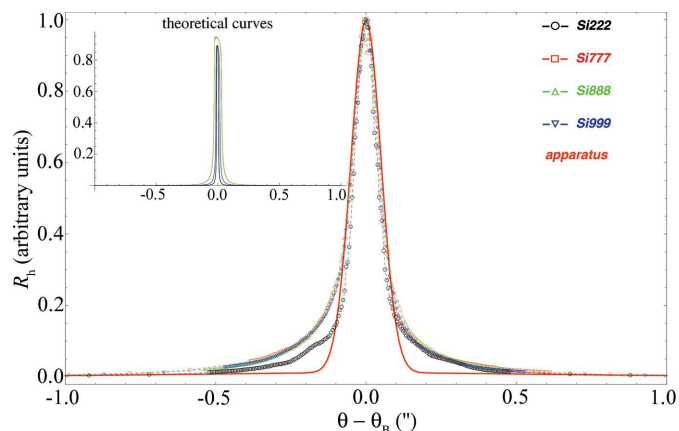


Figure 11

Comparison of the rocking curves obtained from high-order reflections (Si 777, Si 888 and Si 999) and from the Si 222 forbidden reflection together with the apparatus function estimated from the measurements at the lower energy (see Fig. 9). The inset shows the much narrower theoretical reflectivity curves for the different reflections.

with very high quality. The residual strain in the bulk can be in the range of 10^{-8} or even lower (Bonse & Hartmann, 1981). In order to be used as optical elements like a crystal monochromator, the crystals need to be cut into specific shapes (aligned to crystallographic directions) and the surfaces need to be extremely well polished. This is done in different steps that are rather similar in most crystal laboratories, starting with cutting and ending with chemical etching and/or mechanical–chemical polishing (MCP). The typical problem is that the processing of crystals induces lattice deformations (Buck & Meek, 1970; Zhang & Zarudi, 2001) in the form of a cold deformed layer. This layer creates an elastic strain in the crystal region beneath the surface, the strength of which decreases with depth. The thickness of the deformed layer is roughly proportional to the scale of the polishing grains used. Consequently, each processing step removes the deformed layer generated by the previous step, but at the same time it creates a new thinner deformed layer. One manner of removing a deformed layer is to chemically etch it away; however, etching results in a modulation of the surface, known as an ‘orange peel’ surface. Depending on the applications, this modulation may be tolerated or not, *e.g.* for small-angle scattering it needs to be minimized or even avoided. Another way of removing a deformed layer is to use a mechanical–chemical polishing, which uses very small grains and leaves a flatter surface compared to etching.

The anticipated benefit of this part of our work is the improvement of the whole crystal polishing process, and in particular its final steps, using the methods and instruments available at the ESRF. For that purpose one has to measure the crystal bulk and the crystal surface quality. One method to

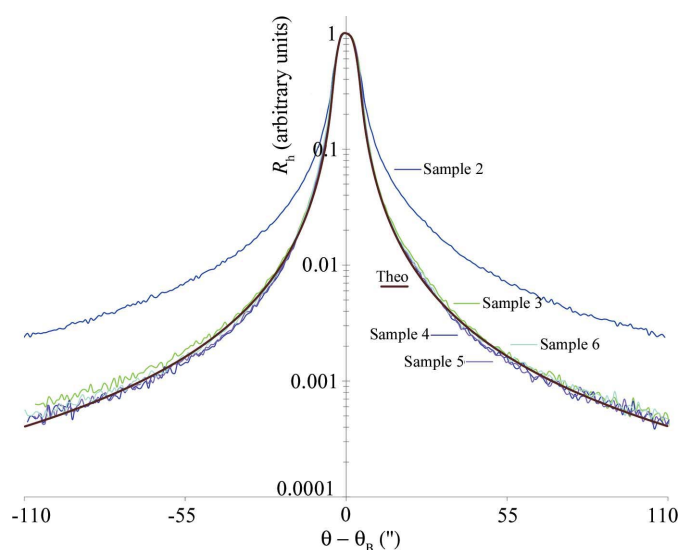


Figure 12 Normalized experimental rocking curves of the Si 111 reflections recorded using a laboratory source of 8.05 keV for a series of silicon samples produced through different processing steps: Sample 2 – optical polishing (1 μm diamond grain); Samples 3–5 – like Sample 2 but in addition one (Sample 3) to three (Sample 5) etching steps of 10 min each; Sample 6 – like Sample 5 with one MCP step between the optical polishing and the chemical etching(s); Theo – theoretical curve for a perfect crystal.

assess whether a crystal is well polished or not is by inspecting it *via* optical microscopy. This method is, however, not sufficiently sensitive for the characterization of Bragg reflecting surfaces to the required standards; hence we adopted for our studies further methods, namely high-resolution X-ray diffraction (local rocking curve measurements), X-ray topography, optical profilometry and atomic force microscopy (Masiello, 2011). Here, we will only focus on metrological aspects and in particular on the possibilities and limits of rocking curve measurements.

An example of the normalized rocking curves referring to the Si 111 reflection for a series of silicon samples (Sample 1 to Sample 6) after different processing steps is shown in Fig. 12. It is clear that the large difference between the rocking curve for the polished Sample 2 and the others is a result of the poor surface state of the latter. However, already after the first etching the different rocking curves become indistinguishable and agree perfectly with the theoretical expectation over a large angular range. Sample 1, which is lapped using 17 μm SiC grains, is shown as line 1 (black) in Figs. 13 and 14.

Slight differences are detected if higher-order-reflection (Si 444) rocking curves are measured using the extremely monochromated beam produced at ID18, at $E = 23.879$ keV with $\Delta\lambda/\lambda = 2.7 \times 10^{-8}$ (see Figs. 13 and 14). In this case it is possible to discern a tiny difference in the tails between Samples 3, 4 and 5. It is also evident that the FWHM as a characteristic parameter is not sufficient for qualifying samples of such high grade. One must inspect the whole curve to extract intrinsic information about the sample. Additional studies *via* X-ray topography show that samples that are not distinguishable at the level of simply the FWHM parameters, even by accurate rocking curve measurements, do, however, show clear differences in the related X-ray topographs (Masiello, 2011).

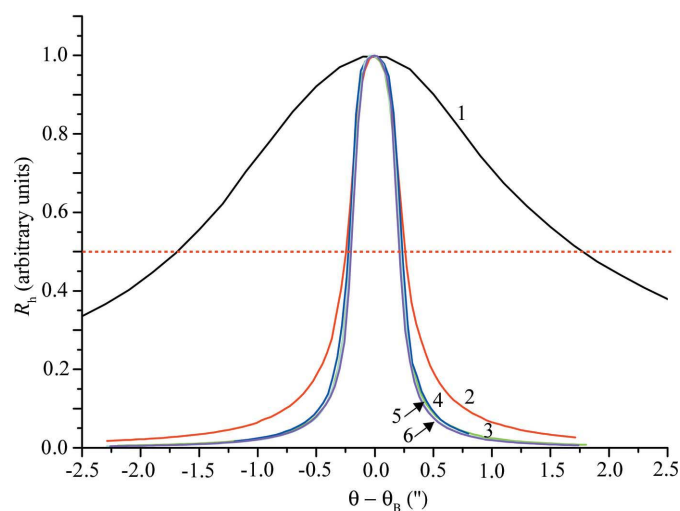


Figure 13 Normalized recorded rocking curves on a linear scale of the 444 reflections at 23.879 keV. Curve 1 (black) is measured as lapped; curve 2 (red) is measured after optical polishing (1 μm diamond grain); curves 3–5 (green, dark blue and light blue) are measured after 10, 20 and 30 min, respectively; curve 6 (purple) is measured after one MCP step between the optical polishing and the chemical etching(s).

5.2. Perfection of different synthetic diamonds

The first synthetic diamond was successfully grown in Stockholm, Sweden, in 1953 using high-pressure and high-temperature (HPHT) processing, but the discovery was kept secret (Lundblad, 1993). One year later, there were two reported diamond syntheses at the General Electric Research Laboratory: one by H. M. Strong and the second by H. T. Hall. The results were quickly published in *Nature* (Bundy *et al.*, 1955) and the method of growing man-made diamond was patented. Those first diamonds were tiny (1.0×0.3 mm) and hardly reproducible. After further experiments, it became clear that to synthesize diamonds a metal ‘solvent/catalyst’ bath would be necessary. In 1971, R. H. Wentorf Jr showed the possibility of growing larger diamonds using the so-called ‘thermal gradient method’ (Wentorf, 1971), which attains the best results in a large-volume belt-press system. With the HPHT method, single-crystal diamonds of more than 1 cm maximum dimension can be grown, and 5–7 mm diamonds with low nitrogen content are routinely grown by companies such as Element Six (formerly De Beers Industrial Diamond) and Sumitomo Electric Industries. An alternative method, the ‘pressure gradient’ method, makes use of a different type of high-pressure system, called a split-sphere BARS press (from the Russian acronym of press-free high-pressure setup ‘split sphere’), to grow large size single crystals (see *e.g.* Pal’yanov *et al.*, 1998).

Another technique used for growing synthetic diamonds is chemical vapour deposition (CVD) (Lee *et al.*, 1999; Ferro, 2002). This is the most widely used technique for depositing many materials in the semiconductor industry, including a wide range of dielectrics and many metals as well as metal alloys. The technique generally involves the growth of a solid material from the gas phase using a reactive gas mixture, which supplies the necessary active species (carbon from

methane in the case of diamond) on a controlled surface (or substrate). The substrate does not have to be diamond, but in order to grow CVD single-crystal diamonds (instead of polycrystalline diamonds) it is necessary to use a diamond substrate with high bulk quality and a high-quality surface finish. The main advantages of CVD techniques are the low pressure needed (consequently a lower cost in terms of equipment), the possibility of growing large diamonds and diamonds on different substrates, and the possibility of introducing dopants in a controlled way during growth. Unfortunately, to date, the quality of the bulk material has not met the requirements for use as X-ray optical elements, even though great improvements were recently made by using high-quality HPHT IIa diamond single crystals as seeds (Martineau *et al.*, 2009).

In summary, one may state that, so far, CVD-grown diamonds may achieve a lower impurity inclusion; however, it is the HPHT synthesis that allows the growth of diamonds with the highest structural quality, *i.e.* crystals that are locally free from extended defects like dislocations and stacking faults. More precisely, the highest quality following this method is achieved for type IIa diamonds, *i.e.* a material with a very low concentration of the (single substitutional) nitrogen impurity, normally less than 1–5 p.p.m. (Chrenko & Strong, 1975). HPHT-grown type IIa diamond crystalline material is also the best suited for the X-ray optical applications we are interested in, *e.g.* high heat load, beam splitter and seeding monochromators for X-ray free-electron laser sources as well as phase plates. If one aims to produce a synthetic diamond where the residual strain arising from the inhomogeneous distribution of nitrogen is less than 10^{-8} then the residual concentration of nitrogen should be less than about 100 p.p.b. (scaling according to Lang’s dilation formula for this impurity; Arridge *et al.*, 2002; Davies, 1999). It is in fact possible to have HPHT-grown type IIa diamond that satisfies this low nitrogen (and boron) concentration requirement.

After evaluating the experimental apparatus function for the setup at ID18, it was possible to estimate the rocking curve broadening due to the presence of defects for different diamond samples. This has been done by using a procedure (model and fit) similar to that presented for the definition/calculation of the apparatus function [see equation (2)].

Table 3 shows a comparison of results obtained for four different typical diamond plates, selected from all the samples analysed. We chose the following samples:

(1) A rather high quality type IIa 100-oriented HPHT-grown diamond plate with a few isolated defects visible on the white beam X-ray topograph and with a very low nitrogen content (about 10 p.p.b.) (measurements using high-sensitivity secondary ion mass spectrometry carried out by the synthesis team for this sample, not published).

(2) A rather high quality type Ib 100-oriented HPHT-grown diamond plate with well advanced growth sectors and growth sector boundaries (nitrogen content typically about 1000 p.p.m.).

(3) A medium-quality 100-oriented CVD-grown diamond plate with well developed dislocation bundles.

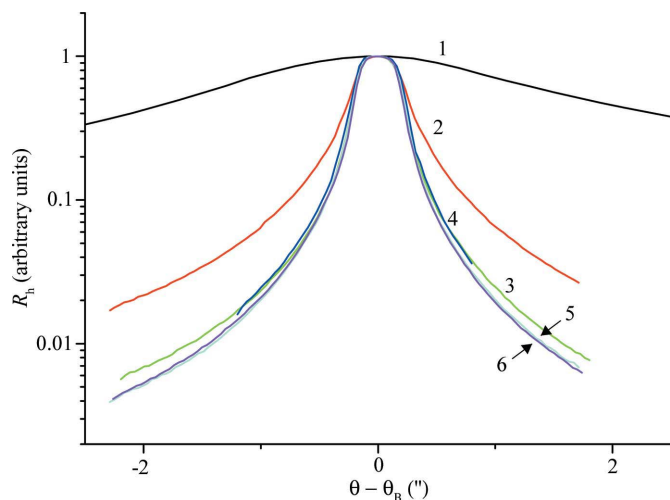

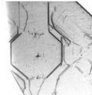
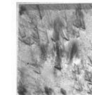
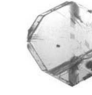


Figure 14 Normalized experimental rocking curves (on a logarithmic scale) of the Si 444 reflections at 23.879 keV. Curve 1 (black) is measured as lapped; curve 2 (red) is measured after optical polishing ($1 \mu\text{m}$ diamond grain); curves 3–5 (green, dark blue and light blue) are measured after 10, 20 and 30 min respectively; curve 6 (purple) is measured after one MCP step between the optical polishing and the chemical etching(s).

Table 3

Extent of rocking curve broadening due to defects, measured at different heights of the rocking curves.

For comparison, the Darwin widths w_h for the used symmetric Bragg reflections 100 and 111 are given. These theoretical values depend slightly on the plate thicknesses. The errors are estimated from the values obtained for the apparatus function at the same height. The bold numbers show very bad values and the italic number a very good value.

	No. 1 (100) IIa	No. 2 (100) Ib	No. 3 (100) CVD	No. 4 (111) IIa
Diamond				
White beam topographs				
Darwin widths (")	1.056	1.129	1.000	2.954
Δ FW50%M (")	<i>0.04</i> (6)	0.86 (6)	0.37 (6)	0.43 (9)
Δ FW20%M (")	0.08 (9)	1.71 (9)	0.74 (9)	0.68 (9)
Δ FW2%M (")	0.28 (15)	3.25 (15)	2.61 (15)	11.96 (15)

(4) A medium-quality type IIa 111-oriented HPHT-grown plate with partly perturbed surface regions.

In order to quantify the broadening of the rocking curve (without comparing the complete shape of the curves), we decided to extract the full width at different peak heights, namely 50, 20 and 2% of the maximum intensity. By doing so one may evidence also the influence of defects on the wings of the rocking curve. For comparison, we also show in Table 3 the intrinsic (theoretical) reflectivity curve widths w_h of the different diamond samples at $E = 14.413$ keV (used energy) for different reflections and different sample thicknesses together with white beam X-ray topographs of the samples to illustrate the defect density of the selected plates.

The results presented in Table 3 show a negligible broadening for Sample 1 in a region close to the centre of the plate. For the Ib sample and the CVD diamond the situation is worse, with a greater broadening recorded at all peak heights. For Sample 4 the results are different. The bulk quality seems good (the theoretical rocking curve is broader for the 111

reflections than for the 400 reflections, and hence the increase of $0.43''$ is relatively small), but the full width at 2% of the maximum is very large. We attribute this to the inferior quality of the plate surface since the 111 surface is the most difficult to polish.

As an example, we present for the first plate in Table 3 some more details regarding the quantitative determination of the 'broadening due to defects', using the intrinsic reflectivity curves and the measured apparatus function. Fig. 15 shows the experimental values (blue circles) compared with the convolution (red line) of the theoretical reflectivity curve, the apparatus function and the broadening due to the defects. The last two were described by the sum of a Gaussian and a Lorentzian function [*cf.* equation (2)]. A very good agreement between the theoretical and measured curves is apparent. In order to compare the widths of the three functions we extracted their FWHM values. We found $1.06''$ for the reflectivity curve (*cf.* Table 1), $0.19''$ for the apparatus function and $0.04''$ for the broadening due to defects. Consequently, we have been able to detect width increases of an experimental rocking curve due to the presence of defects in the diamond plate, which were only a few percent of the curve width itself. This demonstrates that such very small effects are measurable using a carefully planned experimental procedure combined with a very accurate data analysis. This has been a considerable effort, but it has been shown that it is possible to push the used method to an unprecedented upper limit of precision.

6. Conclusion

In order to correctly analyse high-resolution rocking curves of high-grade crystals, a special effort is needed to estimate the systematic contributions coming from the experimental setup. We highlight the main areas that require special treatment and present the results obtained using different approaches to the problem, as well as some typical findings for high-quality silicon and diamond crystals.

The presented results are part of the PhD thesis of one of the authors (Masiello, 2011).

References

- Alkire, R., Yelon, W. & Schneider, J. (1982). *Phys. Rev. B*, **26**, 3097–3104.
- Altin, D., Härtwig, J., Köhler, R., Ludwig, W., Ohler, M. & Klein, H. (2002). *J. Synchrotron Rad.* **9**, 282–286.
- Arridge, R. G. C., Lang, A. R. & Makepeace, A. P. W. (2002). *Proc. R. Soc. London Ser. A*, **458**, 2485–2521.
- Azároff, L. V. (1974). *X-ray Spectroscopy*. New York: McGraw-Hill Book Company.
- Barrett, R., Härtwig, J., Morawe, C., Rommeveaux, A. & Snigirev, A. (2010). *Synchrotron Radiat. News*, **23**, 36–42.
- Berg, W. (1931). *Naturwissenschaften*, **19**, 391–396.
- Bond, W. L. & Andrus, J. (1952). *Am. Mineral.* **37**, 622–632.
- Bonse, U. & Hartmann, I. (1981). *Z. Kristallogr.* **156**, 265–279.
- Bubáková, R. (1962). *Czech. J. Phys. B*, **12**, 776–783.
- Buck, T. N. & Meek, R. L. (1970). *Natl. Bur. Stand. Spec. Publ.* **337**, 419–430.

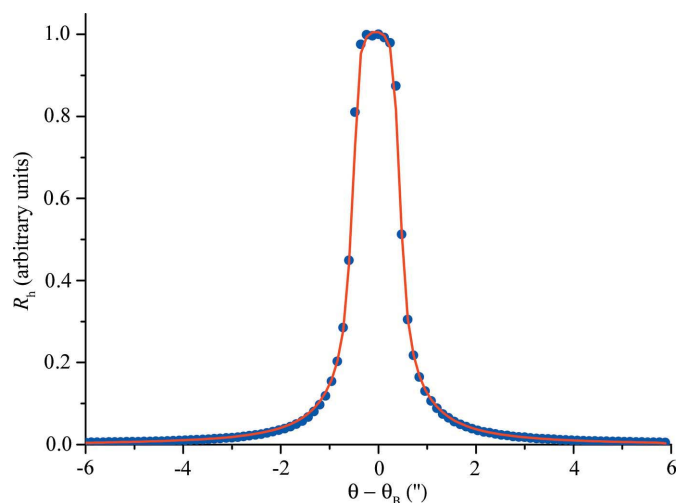


Figure 15

Best fit of experimental values (blue circles) with the curve resulting from the convolution (red line) of the theoretical reflectivity curve, an apparatus function and the broadening due to the defects.

- Bundy, F. P., Hall, H. T., Strong, H. M. & Wentorf, R. H. (1955). *Nature*, **176**, 51–55.
- Burger, H. C. & Van Cittert, P. H. (1932). *Z. Phys. A Hadrons Nucl.* **79**, 722–730.
- Burns, R. C., Chumakov, A. I., Carbone, G., Connell, S. H., Dube, D., Godfried, H. P., Hansen, J. O., Härtwig, J., Masiello, M., Rebak, M., Rommevaux, A., Setshedi, A. R., Van Vaerenbergh, P. & Gibaud, A. (2007). *Proc. SPIE*, **6705**, 67050K1-6.
- Burns, R. C., Chumakov, A. I., Connell, S. H., Dube, D., Godfried, H. P., Hansen, J. O., Härtwig, J., Hozzowska, J., Masiello, F., Mkhonza, L., Rebak, M., Rommevaux, A., Setshedi, R. & Van Vaerenbergh, P. (2009). *J. Phys. Condens. Matter*, **21**, 364224.
- Chrenko, R. M. & Strong, H. M. (1975). Report 75CRD089. Technical Information Series, General Electric Company, Schenectady, NY, USA.
- Darwin, C. (1914). *Philos. Mag.* **27**, 315–333.
- Davies, G. (1999). *Physica B*, **273–274**, 15–23.
- Davis, B. & Stempel, W. (1921). *Phys. Rev.* **17**, 608–623.
- Ferro, S. (2002). *J. Mater. Chem.* **12**, 2843–2855.
- Friedrich, W., Knipping, P. & Laue, M. (1912). *Sitzungsber. K. Bayer. Akad. Wiss.* pp. 303–322.
- Härtwig, J. & Grosswig, S. (1989). *Phys. Status Solidi*, **115**, 369–382.
- Härtwig, J., Hölzer, G., Wolf, J. & Förster, E. (1993). *J. Appl. Cryst.* **26**, 539–548.
- Ida, T., Ando, M. & Toraya, H. (2000). *J. Appl. Cryst.* **33**, 1311–1316.
- Jones, A. F. & Misell, D. L. (1970). *J. Phys. Gen. Phys.* **3**, 462–472.
- Lang, A. R. (1957). *Acta Metall.* **6**, 358–364.
- Lee, S., Lin, Z. & Jiang, X. (1999). *Mater. Sci. Eng.* **25**, 123–154.
- Lucy, L. B. (1974). *Astron. J.* **79**, 745–754.
- Lundblad, L. G. (1993). *High-Pressure Science and Technology – 1993*, AIP Conference Proceedings, Vol. 309, edited by S. C. Schmidt, J. W. Shaner, G. A. Samara & M. Ross, pp. 503–506. New York: AIP Press.
- Martineau, P. M., Gaukroger, M. P., Guy, K. B., Lawson, S. C., Twitchen, D. J., Friel, I., Hansen, J. O., Summerton, G. C., Addison, T. P. & Burns, R. (2009). *J. Phys. Condens. Matter*, **21**, 364205.
- Masiello, F. (2011). PhD thesis, Université de Grenoble, France, http://tel.archives-ouvertes.fr/docs/00/60/92/16/PDF/21831_MASIELLO_2011_archivage_1_.pdf.
- Pal'yanov, Y., Borzdov, Y., Sokol, A., Khokhriakov, A., Gusev, V., Rylov, G. & Sobolev, N. (1998). *Diamond Relat. Mater.* **7**, 916–918.
- Richardson, W. H. (1972). *J. Opt. Soc. Am.* **62**, 55–59.
- Rüffer, R. & Chumakov, A. I. (1996). *Hyperfine Interact.* **97/98**, 589–604.
- Sellschop, J. P. F., Connell, S. H., Nilen, R. W. N., Freund, A. K., Hozzowska, J., Detlefs, C. R., Hustache, Burns, R., Rebak, M., Hansen, J. O., Welch, D. L. & Hall, C. E. (2000). *New Diamond Front. Carbon Technol.* **10**, 253–282.
- Wentorf, R. H. (1971). *J. Phys. Chem.* **75**, 1833–1837.
- Wolfram Research (2009). *Mathematica*. Version 7.0.1. Wolfram Research Inc., Champaign, Illinois, USA.
- Zhang, L. & Zarudi, I. (2001). *Int. J. Mech. Sci.* **43**, 1985–1996.
- Zulehner, W. (2000). *Mater. Sci. Eng. B*, **73**, 7–15.